Contaminant and Heat Removal Effectiveness and Air-to-Air Heat/Energy Recovery for a Contaminated Air Space

Doug R. Irwin, P.E.
Associate Member ASHRAE

Carey J. Simonson, P.E.
Student Member ASHRAE

Kong Y. Saw

Robert W. Besant, P.E.
Fellow Member ASHRAE

ABSTRACT

Measured contaminant and heat removal effectiveness data are presented and compared for a 3:1 scale model room, which represents a smoking room, lounge, or bar with a two-dimensional airflow pattern. In the experiments, heat and tracer gases were introduced simultaneously from a source to simulate a prototype smoking room. High-side-wall and displacement ventilation schemes were investigated, and the latter employed two different types of ceiling diffuser, low-velocity slot and low-velocity grille.

Results show that thermal energy removal effectiveness closely follows contaminant removal effectiveness for each of the ventilation schemes throughout a wide range of operating conditions. The average mean thermal and contaminant removal effectiveness agreed within ±20%. Local contaminant removal effectiveness ranged from a low of 80% for a high-wall slot diffuser to more than 200% for a low-velocity ceiling diffuser with displacement ventilation. Temperature differences between the supply and the indoor air were between 0.2°C (0.36°F) and 41.0°C (73.8 °F) and ventilation airflow rates ranged from 9.2 to 36.8 air changes per hour at inlet conditions. For small temperature differences between supply and exhaust air, all three ventilation schemes showed increased contaminant removal effectiveness near the supply diffuser inlet with decreasing values toward the exhaust outlet. For the high-side-wall slot diffuser, effectiveness was up to 140% near the inlet and 100% near the exhaust, but for the second displacement scheme (low-velocity grille) the effectiveness was more than 200% near the inlet and 110% near the exhaust.

This paper also shows a potential significant reduction in cooling load for a 50-person-capacity smoking lounge that utilizes an air-to-air heat/energy exchanger to recover heat/energy from the exhaust air.

INTRODUCTION

Ventilation of contaminated spaces such as smoking rooms, lounges, and bars for improved air quality and temperature control has become of increasing interest in recent years. The problem is not unlike the problem of the indoor air quality in animal barns where the animals are the prime source of airborne dust and gaseous contaminants that can threaten the health of the animals and especially the people working in the space. In smoking lounges and bars, the primary contaminants are generated by occupant activities (i.e., smoking) and can pose a serious health risk to the occupants, especially the people working in the space. The ventilation design strategy for animal barns is to remove the airborne contaminants as efficiently as practical using 100% outdoor air, avoiding recirculation between rooms, and reducing recirculation within rooms. Irwin and Besant (1994) reviewed the literature and presented data on the ventilation effectiveness and contaminant removal effectiveness of model and full-scale animal barns where 100% ventilation supply air is used for both the removal of contaminants and excess heat. More recently, Hoff et al. (1995) investigated the dispersion of airborne contaminant gases in animal barns that include internal obstructions, while Chen et al. (1995) considered the problem of dust movement and particulate size distribution in animal barns.

The problems of indoor air contamination are usually much less severe in commercial building rooms than in animal barns, resulting in somewhat different design strategies. Heiselberg (1996) notes that the basic principle of ventilation in indoor air spaces is complete mixing to dilute airborne contaminants so that they have an even concentration throughout the space. Heiselberg examined this design objective using a laboratory test facility where the distribution of air exchange and ventilation effectiveness (40% to 150%) were determined for typical room air operating conditions. Heiselberg's

Doug R. Irwin is a performance contracting engineer with Honeywell Ltd., Saskatchewan, Saskatoon, Canada. **Carey J. Simonson** is a graduate student, **Kong Y. Saw** is a student, and **Robert W. Besant** is a professor in the Department of Mechanical Engineering, University of Saskatchewan, Saskatoon, Canada.

research implies that typical operating conditions in rooms often fall short of the design objective for ventilation. Furthermore, since the air in commercial buildings is often recirculated throughout all rooms and there is often considerable direct air exchange between adjacent rooms, cross-contamination between rooms is prevalent.

Chow and Fung (1997) studied airflows and carbon dioxide and tracer gas dispersion in nine different rooms occupied by people. They correlated the local mean age of air and the mean concentration of carbon dioxide with a supply air jet momentum number ($J^* = Q'' U_j$/[g·h]), where Q″ is the supply flow per unit area, U_j is the supply air jet speed, and h is the height of the jet. These data for three-dimensional flows in large rooms show decreased airborne contaminant levels and decreased age of air with increased jet momentum number; however, there is considerable scatter in the data.

In bars or lounges, which permit smoking or the release of airborne contaminants that pose serious health risks to the occupants, especially workers, it is apparent that the conventional commercial building ventilation strategy may be inappropriate. The ventilation strategy for contaminated spaces should be to locate the sources of airborne contaminants near the exhaust grille, isolate the ventilation from any adjacent rooms, and reduce recirculation of air within the space (i.e., displacement ventilation with 100% outdoor air supply). This displacement ventilation should facilitate local mixing to reduce the local concentration of airborne contaminants without significant recirculation within the space. The upstream migration of airborne contaminants should be small. This option is explored herein.

In ventilation studies, it is usually easier and less expensive to measure thermal or sensible energy removal by the air temperature distribution and flow than it is to measure gaseous or aerosol removal by the contaminant concentration distribution and flow of a tracer gas. Further, temperature measurements using thermocouples are often more accurate than contaminant concentration measurements with sampling systems and infrared gas analyzers under typical ventilation study conditions. In cases where significant temperature differences can be introduced, it may be desirable to replace tracer gas studies with temperature studies when investigating the removal of airborne contaminants. Fundamental questions include: when is it valid to use a heat source to replace tracer gas contamination and what accuracy could be expected for such a substitution?

Thermal energy removal effectiveness and ventilation or contaminant removal effectiveness are two measures that can be used to evaluate control strategies for indoor air temperature and indoor air quality. Thermal energy removal effectiveness incorporates differences in temperature between the supply air, exhaust air, and air at different points or zones in the room to assess removal of thermal energy from those points or zones. Similarly, contaminant removal effectiveness makes use of differences in contaminant concentration between the supply, exhaust, and points or zones in the room to evaluate the removal of contaminants from those points or zones. When the source locations for the air contaminants and thermal energy are essentially the same, the temperature distribution and tracer gas concentration distribution data can be expected to be similar.

In this study, the sources for thermal energy and tracer gas contaminant are located at essentially the same place: inside two, two-dimensional cylindrical disturbances that are intended to represent, in a two-dimensional space, tables of people who are smoking. Thermal energy and contaminant removal effectiveness are compared over a range of test conditions for a high-wall slot-inlet and displacement ventilation system with two types of inlet air supply diffusers. Tracer gas (N_2O) is used to simulate airborne contaminants and baseboard heaters are used for heat generation. The airflows induced in the model smoking room are essentially two-dimensional.

THEORETICAL CONSIDERATIONS

Continuity Equations

The basic equations that govern the motion of air in a space of volume, V, and bounded by surface area, A, are the continuity of mass (e.g., air and contaminant species), momentum, and thermal energy. These basic equations may be written at any time, t, for the entire space as integral equations or at any point in the volume as differential equations. The spatial integrals can be found in Panton (1984) and are as follows. For continuity,

$$\int_V \frac{\partial \rho}{\partial t} dv + \int_A \rho(\bar{U} \cdot \hat{n}) da \quad 0, \tag{1}$$

where ρ is the density and $\bar{U}$ is the air velocity. For an airborne contaminant of concentration, C, Equation 1 can be written explicitly for any chemical species or airborne contaminant, C, as

$$\int_V \frac{\partial}{\partial t}(\rho C) dv + \int_A \rho C(\bar{U} \cdot \hat{n}) da = \int_V \rho C''' dv + M/M_c \int_A (\bar{j} \cdot \hat{n}) da, \tag{2}$$

where C''' is the source of strength per unit volume, $\bar{j}$ is the mass flux of contaminant with respect to air, M/M_c is the molecular weight ratio of air to tracer gas, and assuming $C \ll 1$ for each airborne contaminant (e.g., C has typical maximum values of 0.02, 0.004, and 0.0005 for water vapor, carbon dioxide, and respirable aerosol particles, respectively, while minimum values are one or two orders of magnitude smaller). That is, airborne contaminants such as smoke usually have a very small or negligible effect on the air density, ρ, so the bulk motion of the air is not influenced by the existence or concentration of airborne contaminants. An exception to this low concentration of airborne contaminants occurs when there is a large release of gas or vapor (Heiselberg 1996). On the other hand, temperature differences, caused by nonuniform heat sources such as those caused by people and burning cigarettes,

can cause significant buoyancy driven flows, which must be included in the momentum equation. In integral form, the momentum equation is

$$\int_V \frac{\partial}{\partial t}(\rho \bar{U})dv + \int_A \rho \bar{U}(\bar{U}\cdot\hat{n})da = \int_A (\bar{\bar{T}}\cdot\hat{n})da + \int_V \rho \bar{g}dv \,, \qquad (3)$$

which accounts for inertial and buoyancy driven airflows together with viscous drag forces where $\bar{\bar{T}}$ is the stress tensor due to the air pressure and shearing motion and $\bar{g}$ is the gravity vector. The final integral equation is the thermal energy equation:

$$\int_V \frac{\partial}{\partial t}(\rho c_v T)dv + \int_A \rho c_p T(\bar{U}\cdot\hat{n})da = \int_V q'''dv - \int_A (\bar{q}\cdot\hat{n})da + \int_V (\bar{\bar{T}}:\nabla\bar{U})dv \,, \qquad (4)$$

where $\bar{\bar{T}}:\nabla\bar{U}$ $(=\mu\Phi)$ is the viscous dissipation term, c_v and c_p are the specific heats at constant volume and pressure, respectively, $\bar{q}$ is the heat flux vector, and q''' is the heat source strength per unit volume.

The above integral equations for the bulk motion of air can be rewritten at each point in the space in differential form. Here, the common assumptions of incompressible flow, Newtonian fluid, constant properties, Fourier heat flux law, and Boussinesq density-temperature effects are introduced. The resulting equations for continuity, momentum, and thermal energy, written in index form, are at any spatial point (Gebhart et al. 1988):

$$u_{i,i} = 0 \qquad (5)$$

$$u_{j,t} + u_i u_{j,i} = \nu u_{j,ii} - \frac{1}{\rho}p,_j + g_j\beta(T - T_r) \qquad (6)$$

$$T_{,t} + u_i T_{,i} = \alpha T_{,ii} + \frac{\nu}{c_p}\Phi + \frac{1}{\rho c_p}q''' \qquad (7)$$

where u_i is the i velocity component for air, p is the static pressure, ν is the kinematics viscosity of air, β is the thermal coefficient of expansion of air, T_r is the characteristic room air temperature, and α is the thermal diffusivity of air. Introducing Fick's law of contaminant diffusion, Equation 2 becomes, at any point,

$$C_{,t} + u_i C_{,i} = DC_{,ii} + C''' \qquad (8)$$

where D is the mass diffusion coefficient for the contaminant in air.

Equations 5 through 8 apply at each point and are used directly for laminar flows. For quasi-steady turbulent flows, these equations are time averaged at each point, which gives rise to an extra term in each of Equations 6 to 8. These terms account for the turbulent Reynolds stress, heat convection, and mass convection. Research on the turbulent Prandtl number relating momentum and heat transfer in turbulent flows shows that it has a value close to 0.85 in the wake region of boundary layers (Kays 1994), suggesting a close similarity between these transport processes in turbulent flows. Although similar results for momentum and mass transfer are not readily available, they are expected to be the same for turbulent flows.

When the viscous dissipation term Φ can be neglected, which is always the case for laminar flows and some turbulent flows where forced and free convection surface heat transfer effects dominate viscous dissipation, Equation 7 for convective heat transfer and Equation 8 for contaminant mass transfer are similar. This is the case for ventilation in smoking rooms with strong heat sources (i.e., occupants or space heaters) and sinks (i.e., on envelope surfaces). Thus, the dispersion of airborne contaminants at each spatial position in a space is expected to be similar to the dispersion of thermal energy in the same space. Differences can arise, however, due to the location and strength of the sources for heat or airborne contamination. Both Equations 7 and 8 are coupled to the momentum Equation 6 and the continuity Equation 5; however, once the velocity field is known, the motion of the contaminant (C) is determined only by Equation 8. This is not true for air temperature when buoyancy effects are important, as they are for most room airflows, because the last term for buoyancy forces in Equation 6 plays an important role.

Although the analytical problem of solving for the airflow distribution, temperature distribution, and contaminant mass concentration distribution can be formulated (i.e., Equations 5 to 8), provided the initial and boundary conditions are specified, these equations can only be solved for laminar flows. A number of research groups have been working on models for the numerical simulation of turbulent flows in confined spaces such as rooms (i.e., Baker et al. 1994; Kato et al. 1994; and Weathers and Spitler 1993), but the number of assumptions required have usually restricted the results to simple configurations. When the contaminant is introduced directly into an isothermal airspace at various points (not on surfaces), Murakami et al. (1990) showed that for high Reynolds number room airflows in a three-dimensional room of complex geometry with no internal heat sources, measured values of contaminant concentrations deviated from the numerical model by less than 20%. Generally, much more research work is necessary before numerical simulations will be able to accurately predict the behavior of turbulent, buoyant flow in rooms (Chen 1997; Baker et al. 1997) because the turbulent length scales vary spatially throughout typical rooms, suggesting that experimental verification is still required for complex airflows.

Although exact analytical solutions for Equations 5 to 8 are unavailable, the equations provide some insight into the relative importance of the various terms in each equation at any point in a smoking room or lounge. For example, the ratio of inertial to viscous forces in the first term on the right-hand side of Equation 6 results in a characteristic Reynolds number, $Re = U \cdot L/\nu$, while the ratio of buoyancy to inertial forces in the last term on the right-hand side results in the Archimedes

BACK TO PAGE ONE

number, $Ar = g \cdot \beta \cdot \Delta T \cdot h / U^2$. When heat transfer to or from a surface results in buoyancy forces at a point near the surface, buoyancy and viscous forces dominate close to the surface, and the Grashof number, $Gr = g \cdot \beta \cdot \Delta T \cdot h^3 / \nu^2$, best characterizes the airflow and heat transfer.

It is interesting to note the similarity between the Chow and Fung (1997) revised jet momentum number (J^*) and the inverse of the Archimedes number (Ar^{-1}). J^* is the ratio of supply-air jet momentum per unit area of floor ($\rho \cdot Q'' \cdot U_j$) divided by the static air pressure difference between the floor and the supply air jet ($\rho \cdot g \cdot h$), while Ar^{-1} is the characteristic room air momentum per unit flow area ($\rho \cdot U^2$) divided by the characteristic static pressure difference caused by buoyancy effects due to differences in room air temperature over the height of the jet ($\rho \cdot g \cdot \beta \cdot \Delta T \cdot h$). Since Chow and Fung show a good correlation between mean air speed in each room and the supply air diffuser velocity, the difference between J^* and Ar^{-1} is essentially in the selection of static pressure used in the denominator.

Thus, the flow field in a smoking room or bar may best be characterized by a different dimensionless characteristic number or maybe two such numbers at each point in the space. The Reynolds number and revised jet momentum number are expected to be most important for the viscous dispersion of a jet of high momentum. However, if the motion or trajectory of the jet is also determined by buoyancy forces, then the Archimedes number will be important as well as the Reynolds number. At points near surfaces with significant heat fluxes, both the Grashof and Reynolds number may be important, or just the Grashof number may be significant, when inertial effects are induced only by buoyancy forces caused by heat transfer from the surface. For large Reynolds numbers for room airflows, the characteristics of the flow field are expected to be insensitive to small changes in Reynolds numbers, leaving J^* and Ar^{-1} as the most important dimensionless parameters for the flows not adjacent to any surfaces.

Contaminant Removal Effectiveness

Contaminant removal effectiveness, ε, defined as ventilation effectiveness by Heiselberg (1996), is found by injecting tracer gas at typical contaminant source locations and measuring the concentration at various other points including the ventilation exhaust port. Using a constant injection tracer gas technique, contaminant removal effectiveness at any point, p, is determined using the steady-state concentrations at the exhaust (C_e), the supply (C_s), and the point in question (C_p) by

$$\varepsilon_p = (C_e - C_s)/(C_p - C_s) . \qquad (9)$$

Contaminant removal effectiveness will be 100% everywhere for a well-mixed room, less than 100% at points or zones with high concentrations of contaminants, and greater than 100% for points or zones with low contaminant concentrations.

Air exchange effectiveness, on the other hand, is found by injecting the tracer gas into the air supply inlet and measuring the concentration of the tracer gas at the inlet and various points within the space to get the mean age of the air at any point with respect to the nominal mean age of air for the room. Results for air exchange effectiveness are often very similar to contaminant removal effectiveness (Heiselberg 1996). In this study, we only consider the contaminant removal effectiveness or the thermal energy removal effectiveness, as discussed in the next section.

Thermal Energy Removal Effectiveness

The ratio of the temperature difference between the exhaust (T_e) and the supply (T_s) to the temperature difference between any point (T_p) and the supply (T_s) is a measure of the removal of sensible thermal energy at any point relative to the maximum possible cooling potential for a well-mixed space. Using the same form as Equation 9, the thermal energy removal effectiveness (ε_t) at a point, p, is defined as:

$$\varepsilon_{tp} = (T_e - T_s)/(T - T_s) . \qquad (10)$$

Values for ε_{tp} greater than 100% imply an airflow temperature distribution that enhances cooling at the point or zone in question, while values less than 100% imply a poor airflow temperature distribution for cooling at that point or zone.

EXPERIMENTAL EQUIPMENT AND PROCEDURE

To test the similarity of thermal energy and contaminant dispersion, two-dimensional ventilation studies were carried out in a scale model room with a size ratio of about 3:1. This room is equipped with tracer gas injection tubing and baseboard heaters, as described by Irwin and Besant (1994) and shown in Figure 1.

A constant tracer gas technique using nitrous oxide tracer gas was used to simulate contaminants in the model. The baseboard heaters and tracer gas injection tubes in the model were housed within two typical model occupants running the length of the smoking room. The height ratio of these occupants to the room height is 0.224, meaning that the blockage of flow area is very significant but similar to that within lounges that are density occupied. The model occupants were covered in aluminum foil with small infiltration slots along the bottom of each cylindrical contaminant source that allowed air to enter and a single large exfiltration slot along the top center that allowed air and heat to escape into the room. Buoyancy forces between the cylindrical sources and the adjacent room air caused air to flow up through the cylinder carrying both the tracer gas and the heated air into the room space. The smoking room was insulated to reduce conduction, and the aluminum foil reduced radiation so that most of the heat generated within the model occupants was transferred to the space within the room by convection.

To ensure two-dimensional airflow fields within the model room, the ventilation inlets for the slot and displace-

BACK TO PAGE ONE

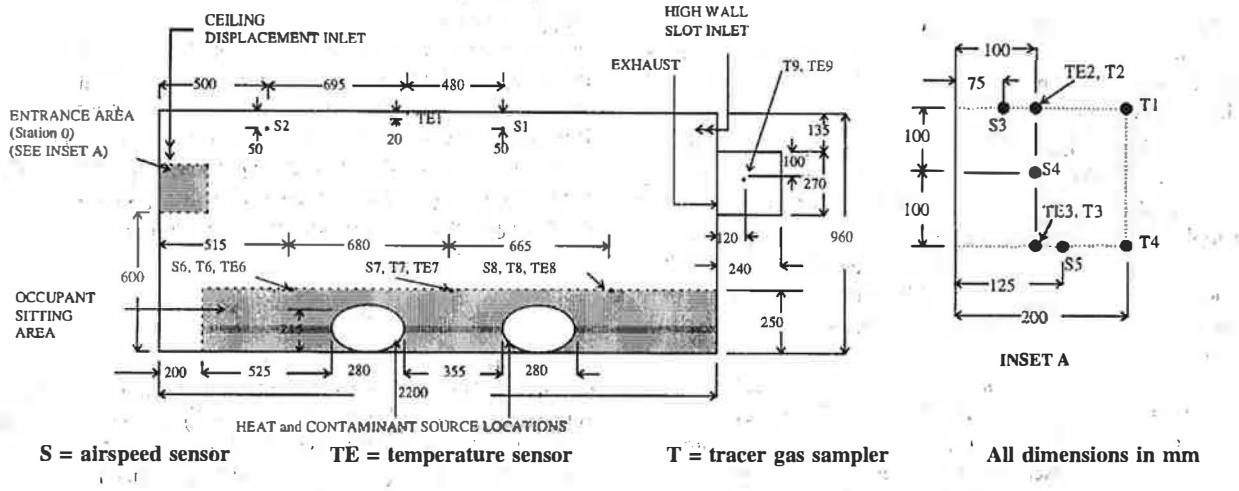

Figure 1 Front view of the model smoking room facility showing the location of heat and contaminant sources, measurement sensors, supply diffusers, and exhaust grilles.

ment ventilation systems ran the entire length of the smoking room. Air was drawn in the room by a single exhaust fan through an exhaust port housing running the length of the room, as described by Irwin and Besant (1994). Airflow patterns were videotaped using a dioctal phthalate (DOP) aerosol particle generator that produced a mist of fine visible particles. The resulting flow visualization patterns using light sheet illumination showed that the airflow fields were virtually two-dimensional over the range of testing; however, the quality of the resulting photos for these turbulent flows was insufficient for proper reproduction and, therefore, they are not included with the data.

The conventional high-wall slot inlet diffuser scheme employed three variable-width slot inlets, as shown in Figure 2. Equal flow rates for each inlet and a constant inlet airspeed of 2.5 m/s (490 ft/min) were retained for each test condition by varying the slot inlet gap. This resulted in a revised jet momentum number, J^*, ranging from 0.007 to 0.027, which is in the same range as the data of Chow and Fung (1997).

The supply air diffuser inlets for the displacement system were positioned over the entrance or bartender to provide fresh outside air to the entrance of the room and bartender. The displacement inlets were designed to result in airspeeds approximately one-tenth of the speeds of the conventional, slot inlet supply jet (i.e., 0.25 m/s [49 ft/min], with the total inlet area approximately 10 times that of the slot inlet system for the same flow rate). These diffuser inlets were covered with a permeable polymer that diffused the incoming air over a large area and created a sufficient pressure drop across the inlets so that backflow from the space to the outside was negligible. This displacement ventilation scheme resulted in a revised jet momentum number 10 times smaller than the slot inlet scheme, or 0.0007 to 0.0027.

In the same manner as the conventional slot-inlet system, the first displacement system used three variable-width slot inlets, as shown in Figure 3. The supply diffuser was located in the ceiling, across the room from the exhaust ports, to induce a displacement flow in the space. The diffuser width

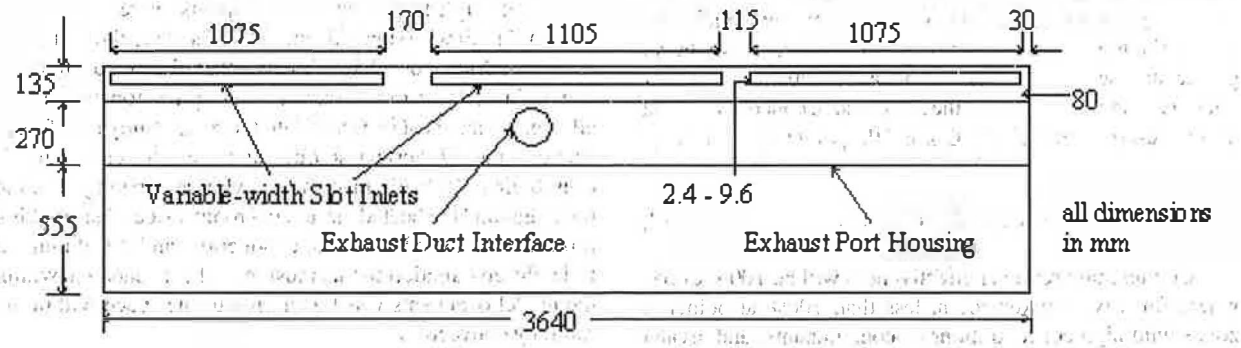

Figure 2 Conventional slot-inlet ventilation system supply-air inlet (side elevation view).

BACK TO PAGE ONE

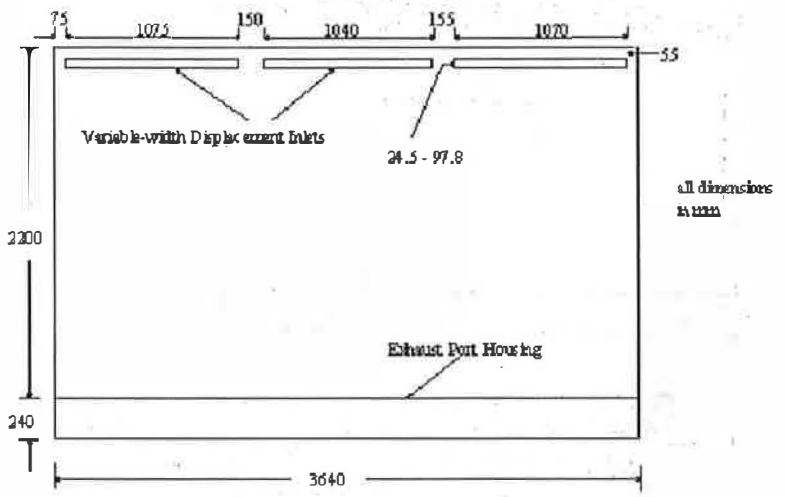

Figure 3 *The first displacement ventilation system supply-air inlets (plan view).*

was varied during testing to retain a constant supply airspeed of 0.25 m/s (49 ft/min) at each diffuser exit.

The second displacement scheme consisted of three series of 12, evenly spaced, supply-air inlets for each group of air inlets, for a total of 36, as shown in Figure 4a. The incoming airspeed for the second displacement system was held constant at 0.25 m/s (49 ft/min) for each flow rate by varying the number of open supply-air inlets. The inlets were either completely opened or closed. Four ventilation rates per unit floor area were investigated at entrance conditions for the second displacement ventilation system, i.e., 2.46, 4.91, 7.36, 9.82 L/(s·m^2) (0.48, 0.97, 1.45, 1.93 cfm/ft^2), based on the entrance air density. For the other two ventilation systems, a rate of 3.68 L/(s·m^2) (0.72 cfm/ft^2) was also investigated. For the highest flow rate, 9.82 L/(s·m^2) (approximately 36.5 ACH at inlet conditions), all the inlets were opened. For the other flow rates, a number of inlets were closed to result in the same inlet air speed for each test. For 2.46 L/(s·m^2) (approximately 9.1 ACH at inlet conditions), 9 inlets were opened; for 4.91 L/(s·m^2), 18 inlets were opened; and for 7.36 L/(s·m^2), 27 inlets were opened, as shown in Figure 4b.

Tracer gas measurements were made using N_2O tracer gas and an infrared gas analyzer with a sensor error of less than 2 ppm over the measured range from 30 ppm to 180 ppm. Temperatures were measured using T-type thermocouples with an error of less than 0.2°C (0.36°F). The results are presented in the form of contaminant and thermal energy removal effectiveness. Contaminant and temperature measurements were made at six corresponding points in the smoking room, as shown in Figure 1. Instrumentation for the two types of measurements, thermocouples with supports and tracer gas sampling tubes, were placed in two distinct cross sections, 100 mm (4 in.) apart, to minimize airflow distribution interference between the probes.

For each test, the system was allowed to reach quasi-equilibrium before measurements were taken. Equilibrium was determined by monitoring temperatures, without recording, in the room and the exhaust tracer gas concentration. When there was little change in both temperatures and exhaust concentration for at least 15 minutes, testing was started. At least two hours passed between a change in test conditions (i.e., flow rate or heat generation level) and the beginning of the next set of data collection. Temperature differences between the supply and the indoor air were from 0.2°C (0.36°F) to 41°C (73.8°F) for heat inputs of 500 W (1700 Btu/h) to 2000 W (6825 Btu/h) (i.e., 62.5 W/m^2 [20 Btu/(h·ft^2)] to 250 W/m^2 [80 Btu/(h·ft^2)].

Tracer gas concentrations were monitored at eight points in the smoking room, as shown in Figure 1. Points 1 through 4 are in the operator area, points 6 through 8 are in the occupant area, and point 9 is in the exhaust. For each region, contaminant removal effectiveness (ε) was found by averaging the effectiveness obtained at each point within each region, i.e., the entrance region, where the contaminant removal effectiveness is expected to be high, and the client-occupied region, where the contaminant removal effectiveness is expected to be good but not as high as the entrance region. Temperatures were measured at the seven points shown in Figure 1. Points TE2 and TE3 are in the entrance area, points TE6, TE7, and TE8 are in the occupant area, and point TE9 is in the exhaust. Supply air temperatures were measured with a mercury thermometer, and all other temperatures were measured by T-type thermocouples that were shielded to reduce radiation errors. Thermal energy removal effectiveness (ε) for each region was found by averaging the effectiveness obtained at each point within the region. For the calculation of the room effectiveness, point TE1 at the ceiling was not used since it was too far from the occupied area.

BACK TO PAGE ONE

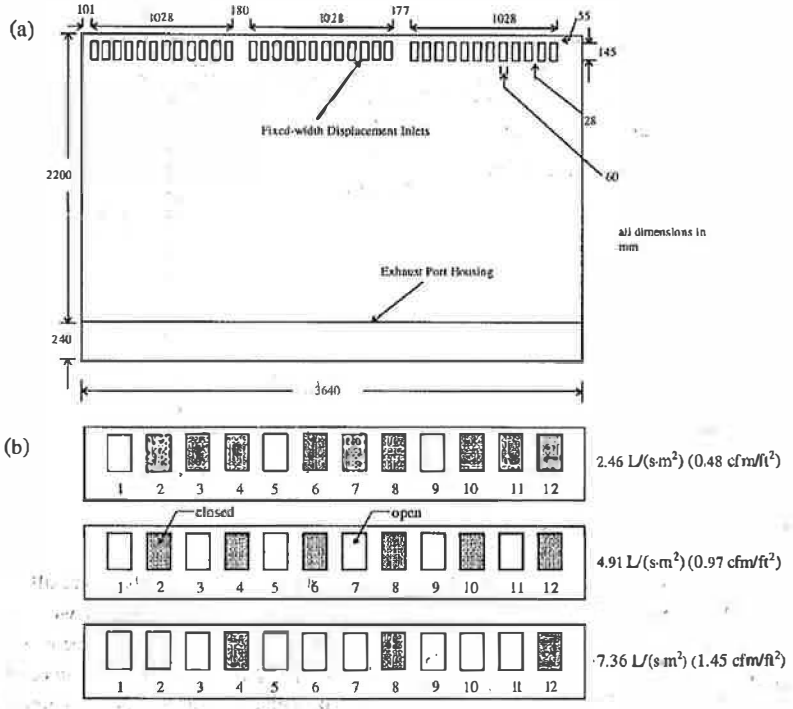

Figure 4 Plan view of the second displacement ventilation system showing (a) the supply-air inlets and (b) the opening sequence of the supply-air inlets.

EXPERIMENTAL RESULTS AND DISCUSSION

The graphical results for effectiveness are, in most cases, presented as a function of temperature difference in °C. This dimensional temperature difference can be interpreted physically as directly proportional to the product of the Archimedes number (Ar) and the revised jet momentum number (J^*), which has a range of 0.03 ΔT to 0.2 ΔT for the range of data used here where ΔT has the units of °C. The results are presented so that direct comparisons can be made between contaminant and thermal energy removal effectiveness for each test.

Contaminant Removal Effectiveness

Figure 5 shows the contaminant removal effectiveness results obtained in the room and occupied areas of the model smoking room with the slot-inlet and the first and second displacement ventilation schemes. The maximum absolute error in contaminant removal effectiveness was 27.5%; however, the maximum relative error as a percentage of the contaminant removal effectiveness value was 7.6%.

As Figure 5a illustrates for the high-wall slot inlet diffuser, entrance area contaminant removal effectiveness ranged from about 80% to just over 110%, while contaminant removal effectiveness in the occupant area ranged from about 100% to 110%. These results are similar to those for conventional ventilation air mixing (Heiselberg 1996; Chow and Fung 1997).

The displacement ventilation systems (Figures 5b and 5c) show a decline in contaminant removal effectiveness with increasing temperature differences and decreasing mass flow rates. In the entrance area, the contaminant removal effectiveness for the first displacement system was relatively steady at about 100%, which is lower than the effectiveness obtained with the slot-inlet system at the higher flow rates (7.36 and 9.82 L/(s·m²). This low effectiveness was caused by the low-speed entrance jet attaching to the wall and essentially bypassing the sensors shown in Figure 1. The second displacement system entrance area contaminant removal effectiveness ranged from about 100% to 365%, always equal to or higher than the contaminant removal effectiveness in the same region for either the slot-inlet or the first displacement systems. Contaminant removal effectiveness in the occupant area for the two displacement systems was higher under all conditions than for the conventional high-wall slot-inlet system. Occupant area contaminant removal effectiveness for the two displacement systems was similar except at the highest flow rate of 9.82 L/(s·m²), where the second displacement system was 20% more effective. Occupant area effectiveness for the displacement systems ranged from about 120% to 155% for the first system and from 115% to 175% for the second system, increasing with flow rate and decreasing with heat generation rate.

BACK TO PAGE ONE

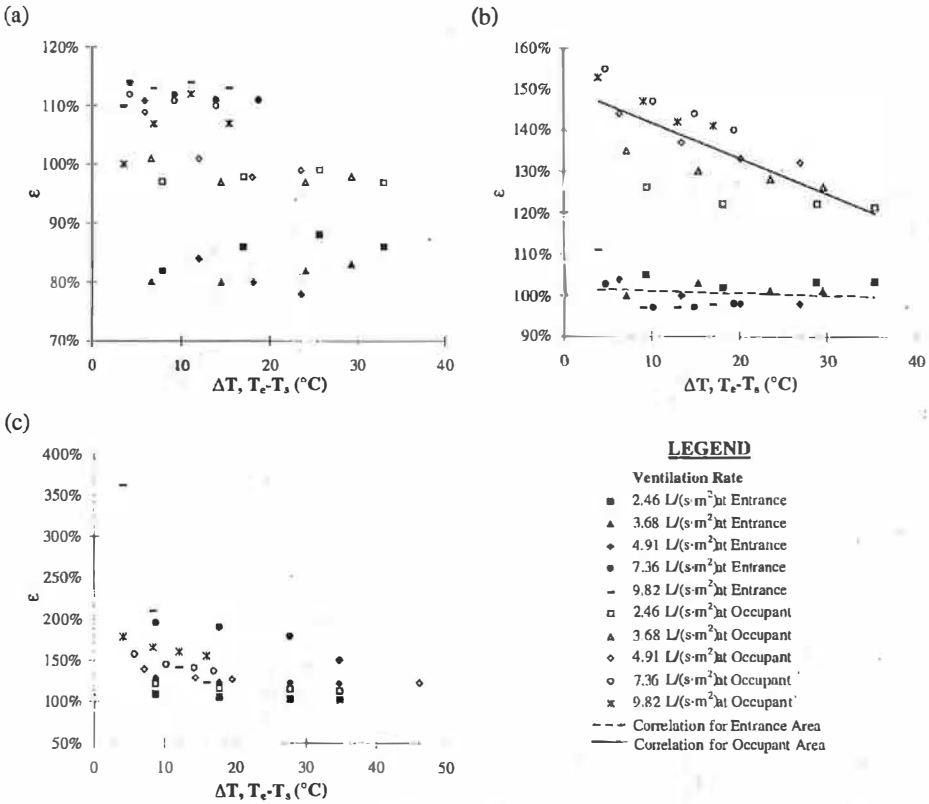

Figure 5 *Entrance and occupant area contaminant removal effectiveness for the (a) slot-inlet, (b) first displacement, and (c) second displacement ventilation schemes.*

Thermal Energy Removal Effectiveness

Thermal energy removal effectiveness data for the slot-inlet and the first and second displacement systems are plotted in Figure 6 for the entrance and occupant areas. The maximum relative error in thermal energy removal effectiveness as a percentage of the thermal energy removal effectiveness value was 105.5%; however, the median relative error was less than 5%.

The thermal energy removal effectiveness data follow the same trend as the contaminant removal effectiveness data. As with the contaminant removal effectiveness data, a transition is evident at the 4.91 L/(s·m^2) flow rate and a heat rate between 500 W (1700 Btu/h) and 1000 W (3410 Btu/h) or 62.5 W/m^2 (20 Btu/[h·ft^2]) and 125 W/m^2 (40 Btu/[h·ft^2]). The transition is particularly evident in the entrance area data of Figure 6a. These results are similar to the contaminant removal results in Figure 5a. This transition was accompanied by a change in the airflow pattern, as the supply air jet did not reach the opposite wall for the higher heat rates, resulting in lower values of ε_t. Similar two-dimensional flows, with short-circuiting of the ventilation air when buoyancy is important, were reported by Zhang et al. (1992).

The first displacement system results show that thermal energy removal effectiveness increased with increasing flow rate and decreasing temperature differences. Unlike contaminant removal effectiveness, thermal energy removal effectiveness for the occupied zones with the first displacement system did not show distinct differences in trends between the zones. They were nearly equal in magnitude, and both increased as the ΔT decreased (Figure 6b).

Thermal energy removal effectiveness for the second displacement system follows the same trend as contaminant removal effectiveness, increasing with decreasing temperature difference and increasing flow rate, as shown in Figure 6c. However, the extremes of the data are exaggerated for thermal energy removal effectiveness, ranging from 100% to 410%. The extremely high effectiveness of 410% has a large experimental uncertainty of ±52%. Thus, the high effectiveness at that point and the very large difference compared to contaminant removal effectiveness may be mostly due to experimental error.

In general, the thermal energy removal effectiveness data are similar to the contaminant removal effectiveness data, as shown in Figure 6. This finding is expected because the physical process for the removal of warm air is the same as for the removal of airborne contaminants when buoyancy effects are small. In ventilation investigations, where the air contaminant and heat sources are together (as is often the case with people,

BACK TO PAGE ONE

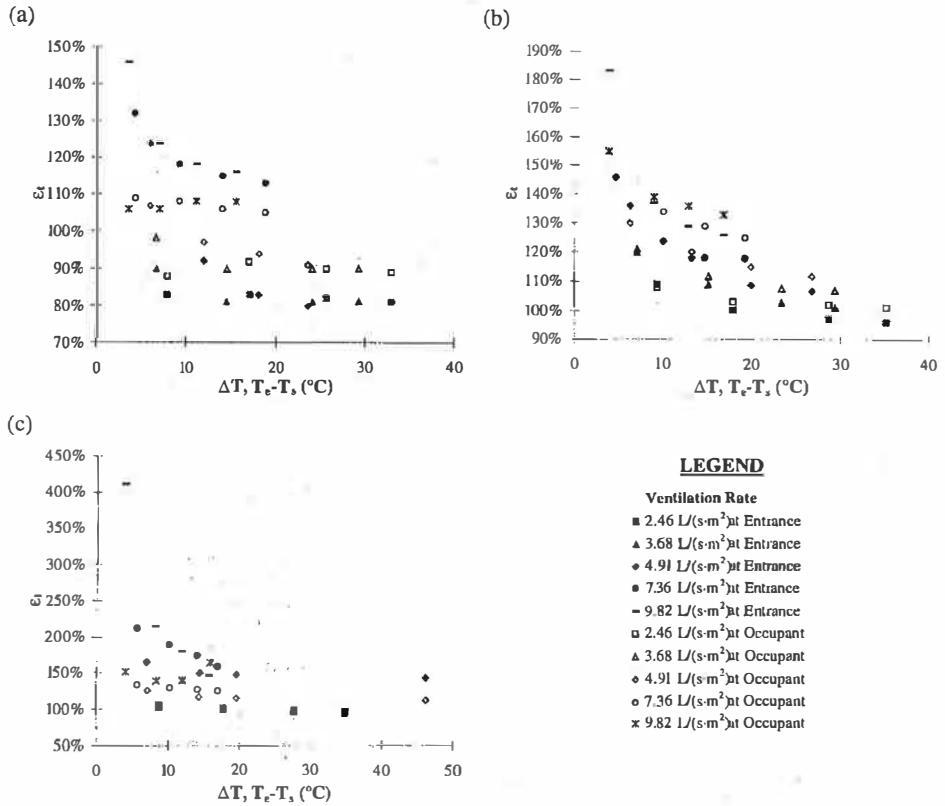

Figure 6 *Entrance and occupant area thermal energy removal effectiveness for the (a) slot-inlet, (b) first displacement, and (c) second displacement ventilation scheme.*

cigarette smoke, animals, and some industrial processes with strong heat sources), and where there are significant temperature differences within the space, thermal energy may be used in the same manner as tracer gases. Using thermal energy could greatly simplify these investigations since low-cost thermocouples are readily available to measure temperatures, whereas gas analyzers to measure gas concentrations are costly and relatively inaccurate without frequent and careful calibration. On the other hand, there are limitations in calculating thermal energy removal effectiveness because large uncertainties occur with small air temperature differences. As the temperature difference decreases, the relative error in the thermal energy removal effectiveness increases.

Figure 7 directly compares the measurements of contaminant removal and thermal energy removal effectiveness for each measurement point in the space.

Figures 7a, 7b, and 7c clearly indicate a strong correlation between the two types of effectiveness over a wide range of test conditions. If the entrance and occupant conditions had been combined as single data points in Figure 7, the agreement between the two types of effectiveness would show even less discrepancy. Comparing contaminant and thermal energy removal effectiveness at each point in Figure 7 shows that the two types of effectiveness are similar, although significant discrepancies exist. The precision of the correlated data (tSEE) in Figure 7 ranged from 18% to 43% for the occupant space and 30% to 84% for the entrance region, suggesting moderately good agreement for the occupied spaces but poor agreement for the entrance region in spite of the good correlation coefficients, except for the entrance region of the first displacement ventilation scheme (Figure 7b). This lack of good agreement in the entrance region is due in part to the slightly different configuration for contaminant and temperature sensors, as shown in Figure 1.

A negative bias in the entrance region of the first displacement and slot-inlet system indicates that the entrance region temperatures are lower than expected for good agreement between thermal energy removal effectiveness and contaminant removal effectiveness. The higher errors in the thermal energy removal effectiveness data in the entrance area for the second displacement system make drawing conclusions from these data difficult. These high errors are due to the small temperature differences in the entrance region. For all of the systems, the occupant area data show a slightly positive bias, indicating that the temperatures are slightly higher than expected for a good match of the two types of effectiveness. The exception is for the slot-inlet system at point T6/TE6, where a slightly negative bias is seen. This negative bias occurs for the thermal energy removal effectiveness for 500 W (1700 Btu/h) (i.e., 62.5 W/m^2 (20 Btu/[h·ft^2]) heat input and

BACK TO PAGE ONE

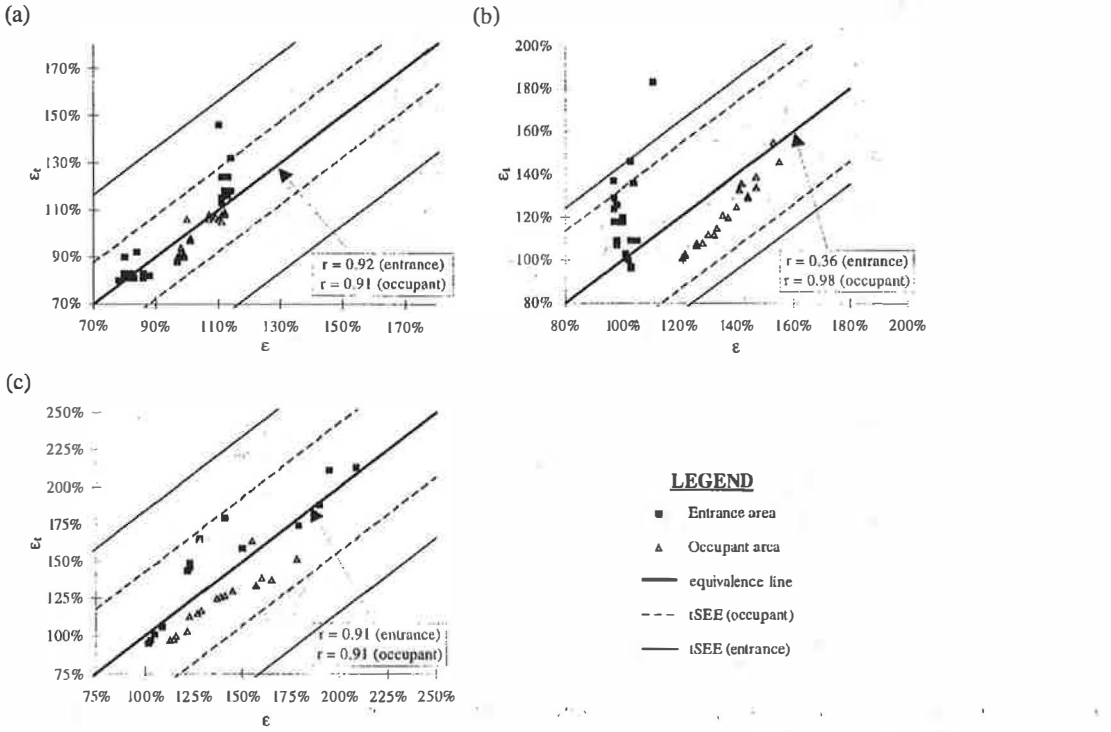

Figure 7 *Contaminant (ε) and thermal energy (ε_t) removal effectiveness for the (a) slot-inlet, (b) first displacement, and (c) second displacement ventilation scheme.*

flow rates of 7.36 L/(s·m^2) (1.45 cfm/ft^2) and 9.82 L/(s·m^2) (1.93 cfm/ft^2). The uncertainty in thermal energy removal effectiveness at these conditions is very high because the temperature differences are small.

Although radiation shields were incorporated for both the heat sources and the thermocouples used at each station, the slight mean bias errors in the effectiveness data can be partly attributed to thermal radiation. Radiation from the model occupants is larger in the occupant region then the entrance region (resulting in slight biases in temperature measurements), higher in the occupant region, and lower in the entrance region. Radiation errors decrease as the airspeed increases because convective heat transfer is directly related to the airspeed. This explains the higher bias in the first displacement system, where the measured airspeeds were usually two to three times lower than for the other systems, and also the high bias in the occupant region for the second displacement system, where airspeeds were also very low.

In the measurement of tracer gas concentrations, errors may occur due to sampling location and duration as well as the magnitude, particularly at low concentrations. Furthermore, longer time constants are required for tracer gas sampling systems than for temperature measurements. Although unsteady effects were not a factor in this experiment, they could be a factor in field tests where tracer gas system transient effects could cause error.

Figure 8 illustrates the variation in effectiveness with distance from the entrance area where Station 0 is the entrance area and Stations 6, 7, and 8 are progressively farther from the entrance area and closer to the exhaust.

Figure 8 shows the thermal energy removal effectiveness vs. temperature difference for each measuring station in the occupied region. This figure clearly shows that small temperature differences and closeness to the entrance region lead to substantially improved effectiveness, while large temperature differences and locations near the exhaust outlet lead to effectiveness close to 100%, or the same as a well-mixed room. Using the correlations from Figure 8, Figure 9 shows the thermal energy removal effectiveness vs. distance from the entrance region wall for the slot and the two displacement ventilation schemes. The results in Figures 8 and 9 are expected to apply for contaminant removal as well, which means that staff in a smoking lounge can have significantly reduced exposure to contaminants if their work location is near the supply air inlets and 100% outdoor air is supplied in a displacement ventilation scheme.

AIR-TO-AIR HEAT/ENERGY RECOVERY

The purpose of this section is to investigate the potential for air-to-air heat/energy recovery in smoking rooms, bars, and lounges. According to *ANSI/ASHRAE Standard 62-1989*, a smoking lounge requires an outdoor ventilation rate of 30 L/

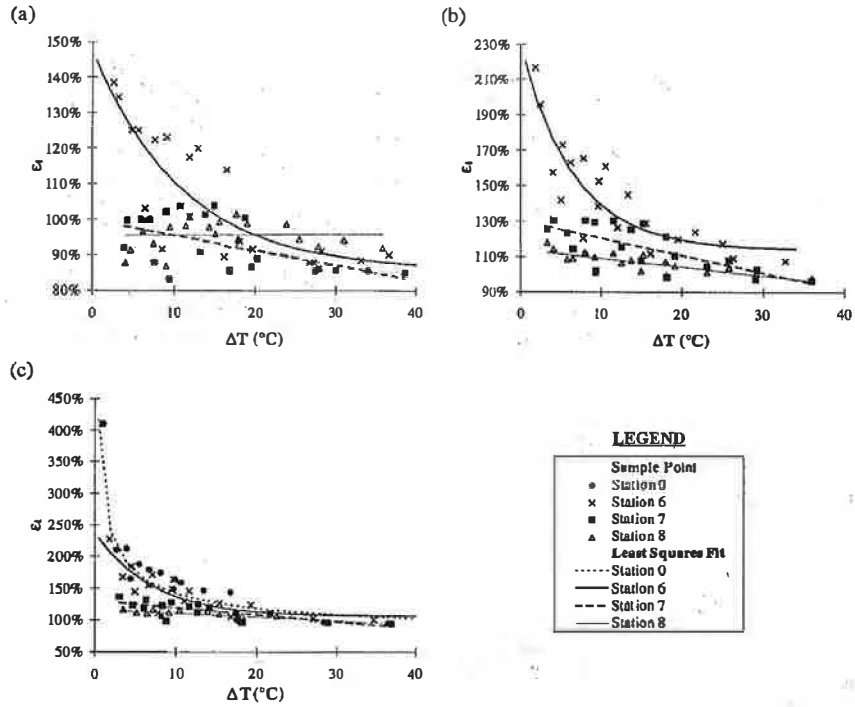

Figure 8 *Local thermal energy removal effectiveness (ε_t) for the (a) slot-inlet, (b) first displacement, and (c) second displacement ventilation scheme.*

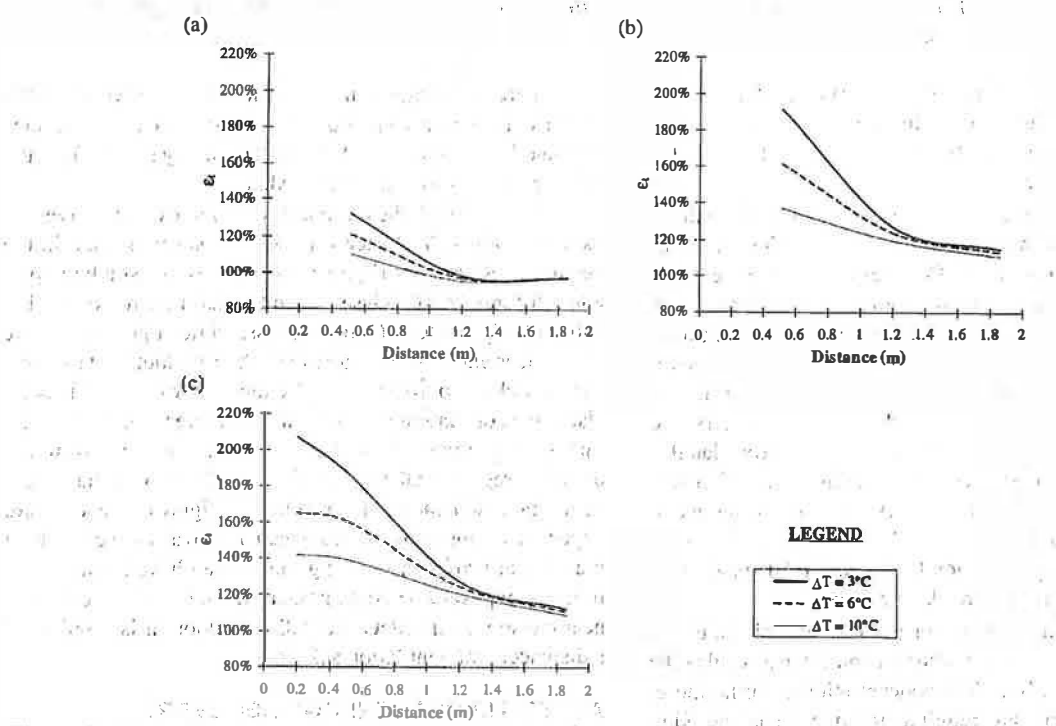

Figure 9 *Thermal energy removal effectiveness (ε_t) vs. distance from the wall opposite to the exhaust for various differences between the local temperature and the supply temperature for the (a) slot-inlet, (b) first displacement, and (c) second displacement ventilation schemes.*

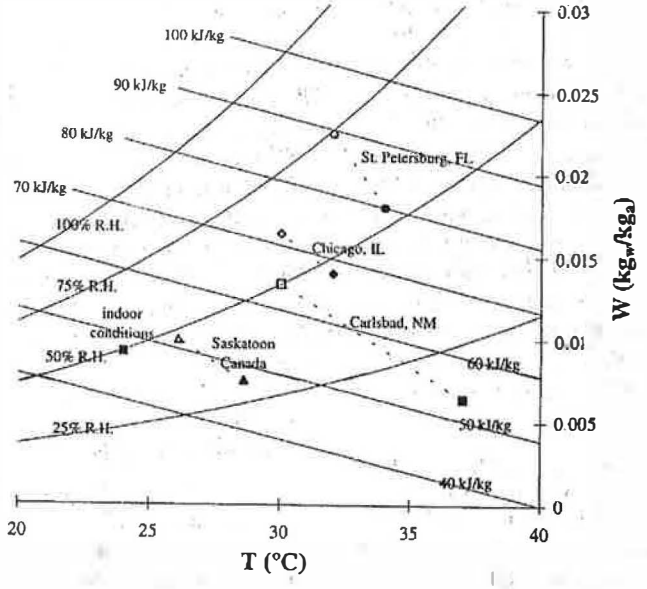

Figure 10 *The 1% outdoor summer design conditions on the psychrometric chart. The open symbols represent the wet-bulb and mean coincident dry-bulb temperatures (WB/MDB) and the filled symbols represent the dry-bulb and mean coincident wet-bulb temperatures (DB/MWB).*

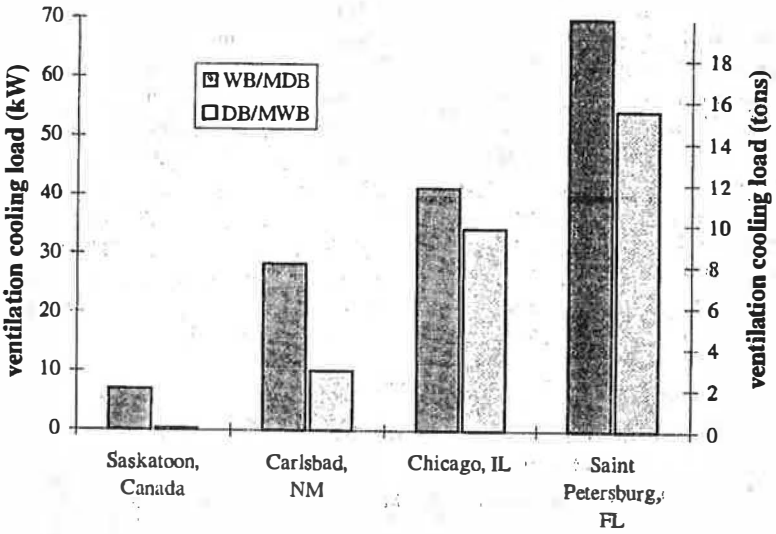

Figure 11 *Ventilation cooling loads for a 50-person-capacity lounge in various locations.*

(s·person). For a moderately sized lounge that is designed for 50 people (i.e., 16 to 25 times the floor area [scale factor 4 to 5] of the laboratory test facility used to investigate ventilation effectiveness in this paper), the outdoor ventilation rate is 1500 L/s (3000 cfm), which corresponds to the highest airflow rate investigated for ventilation effectiveness (i.e., ≈ 10 L/[s·m^2] [2 cfm/ft^2]). Using the 1% summer design conditions shown in Figure 10 (ASHRAE 1997), the ventilation cooling load for a 50-person-capacity smoking lounge located in four different cities is given in Figure 11. The ventilation cooling load in Figure 11 is calculated using

$$\text{ventilation load} = \dot{m}\Delta H, \tag{11}$$

where $\dot{m}$ is the mass flow rate of dry air and ΔH is the enthalpy difference between the indoor and outdoor air. The summer outdoor design conditions are taken as the 1% annual cumulative occurrence wet-bulb temperature and the mean coincident dry-bulb temperature (WB/MDB) and the traditional 1% annual cumulative occurrence dry-bulb temperature and the mean coincident wet-bulb temperature (DB/MWB). The indoor conditions are assumed constant at 24°C and 50% relative humidity.

Figure 11 shows that the ventilation cooling load is always greater for the WB/MDB design conditions than for the DB/MWB design conditions. With the WB/MDB design conditions, the ventilation load for the lounge is substantial and ranges from 6.9 kW (2.0 tons) in Saskatoon, Canada, which has a cool and dry climate, to 70.1 kW (19.9 tons) in Saint Petersburg, Fla., which has a hot and humid climate. It is interesting to note that the design cooling load is greater in Chicago, Ill., than in Carlsbad, N. Mex., for both design conditions even though the climate in Carlsbad is hotter than the climate in Chicago. The reason for this is that the enthalpy of the outdoor air at design is higher in Chicago. This means that when the weather is hot in Carlsbad, the humidity is typically low, which shows the importance of latent energy on the cooling of ventilation air.

The potential energy savings and chiller capacitance reductions that air-to-air heat/energy recovery devices could achieve in this 50-person-capacity smoking lounge will be estimated in this example for both a sensible heat exchanger and a total energy exchanger. The sensible heat exchanger will be assumed to transfer only sensible energy (i.e., no condensation), and the total energy exchanger will transfer both sensible and latent energy. The sensible effectiveness of a well-designed sensible heat exchanger (e.g., heat pipe, flat plate, or run-around heat exchanger) is typically about 60% to 75% (Johnson et al. 1998, 1995; ASHRAE 1996). A well-designed energy exchanger (i.e., energy wheel) can have total energy effectiveness in the range of 65% to 75% (Simonson et al. 1998; ASHRAE 1996). In this analysis, it will be assumed that the sensible heat exchanger has a sensible effectiveness of 70% and the energy wheel has a total effectiveness of 70%. For simplicity, the effectiveness will be considered constant regardless of the operating conditions, which is not exactly correct for actual air-to-air heat/energy exchangers (Simonson and Besant 1997, 1998; Johnson et al. 1998). When an energy wheel is used to recover energy from the exhaust air, the amount of outdoor ventilation air should be slightly greater than that specified in *ANSI/ASHRAE Standard 62-1989* to ensure proper indoor air quality because the wheel rotation will result in carry-over leakage between the supply and exhaust airstreams. In addition, energy wheels are more susceptible to cross-leakage than other heat exchangers. In this example, the outdoor ventilation airflow is increased by 10% when the energy wheel is used to account for these potential leakages. This means that the carry-over and cross-leakages are assumed to be 10% of the supply airflow rate, which is slightly greater than that measured by Johnson et al. (1998) and Simonson et al. (1998). Figure 12 shows the potential load savings that air-to-air heat/energy exchangers create when they are used to precondition the supply air at design conditions for various locations.

Figure 12 shows that savings in cooling energy are significant in nearly all cases. The reduction in cooling energy is the greatest in Saint Petersburg, where the reduction in required cooling capacity is 47 kW (13.4 tons) for the 1% wet-bulb design temperature and the mean coincident dry-bulb temperature (WB/MDB). The savings that would result from this chiller capacity reduction would result in an immediate payback for the air-to-air energy recovery system if it was installed during initial construction or during a chiller retrofit. The decrease in required chiller capacity for a lounge located in Saskatoon, Carlsbad, and Chicago would be 4.6 kW (1.3 tons), 19.0 kW (5.4 tons), and 27.7 kW (7.9 tons), respectively. A decrease in the required chiller capacity could also be important because replacing R-11 with more environmentally friendly refrigerants could result in a reduction in chiller capacity. If the change in refrigerant is accompanied with the retrofit of an air-to-air heat/energy exchanger, the cooling capacity of the system could be kept the same or could even possibly be increased.

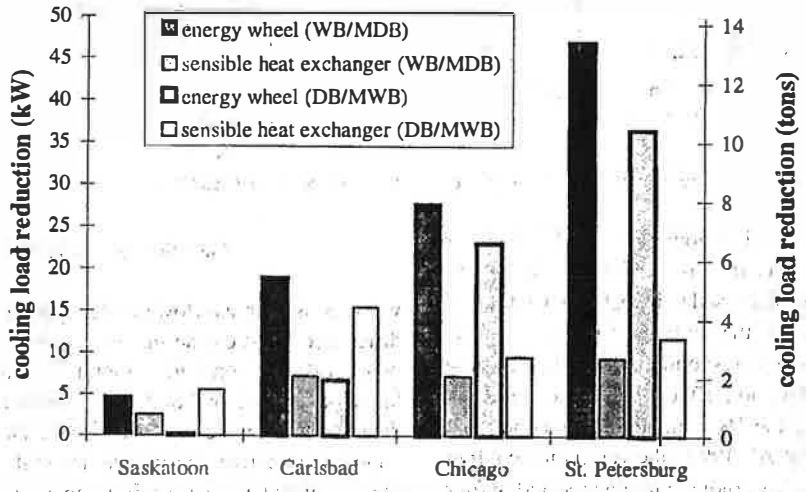

Figure 12 *Reduction in cooling load that results from using an energy wheel or a sensible heat exchanger to precondition ventilation air for a 50-person-capacity lounge.*

BACK TO PAGE ONE

Figure 12 shows an important difference between the WB/MDB design condition and the more traditional DB/MWB design condition as they apply to ventilation air energy recovery. When using the WB/MDB design condition, the energy wheel provides a greater reduction in chiller capacity than the sensible heat exchanger for all locations. However, when the traditional DB/MWB is used as the design condition, the energy wheel is favorable in Chicago and Saint Petersburg, but the sensible heat exchanger is favorable in Saskatoon and Carlsbad. This shows that in order to make a correct decision regarding air-to-air heat/energy recovery, hourly weather data should be used with building simulation packages to choose the exchanger that will give the greatest reduction in chiller capacity and cooling energy, while having the least life-cycle cost. The results in this brief example show that an energy wheel is favorable when the outdoor humidity is high because it can transfer both sensible and latent energy; whereas, a sensible heat exchanger is favorable when the outdoor humidity is low (i.e., outdoor humidity ratio less than indoor humidity ratio) and the latent heat transfer is small.

SUMMARY AND CONCLUSIONS

The objective of this research was to compare contaminant removal effectiveness and thermal energy removal effectiveness in the occupied zones of a heated scale-model smoking room, lounge, or bar, and to investigate the potential for using air-to-air heat/energy recovery to reduce the cooling load of such rooms. To do this, a model smoking room was fitted with a conventional high-wall, slot-inlet diffuser and two low-velocity ceiling diffusers for displacement ventilation. Heat and tracer gases were generated in two, two-dimensional model occupants in the smoking room. Temperatures and tracer gas concentrations were monitored at corresponding points in the model smoking room with thermocouples and tracer gas sampling tubes and an infrared gas analyzer. Effectiveness results were calculated from the measured data for each of the ventilation systems and compared.

Results show:

1. Airborne contaminant and thermal energy dispersion and advection in rooms are similar when the contaminant and heat source locations are the same and buoyancy effects are small (e.g., contaminant and thermal energy removal effectiveness generally agree within ±15%; however, differences as large as 58% for a particular test condition and location can occur).
2. Compared to a well-mixed space, significant improvements in the contaminant and thermal energy removal effectiveness were observed for the three ventilation schemes investigated, especially the displacement schemes.
3. Discrepancies between the effectiveness of contaminant and thermal energy removal due to radiation effects on the temperature sensors and small temperature differences should be minimized, as discussed herein, when airborne temperature dispersion and advection studies are used to replace tracer gas studies.
4. Air-to-air heat/energy recovery devices greatly reduce the cooling load and needed chiller capacity for smoking lounges, with energy wheels providing a greater reduction in chiller capacity than sensible heat exchangers, especially when the climate is warm and humid.
5. Chiller capacity reductions were as high as 47 kW (13.4 tons) for a 50-person-capacity smoking lounge in Saint Petersburg, Fla.

NOMENCLATURE

a = surface area (m^2)
A = characteristic area (m^2)
C''' = contaminant source strength per unit volume (m^3/[m^3·s])
C = air contaminant concentration (volume fraction in ppm)
DB/MWB = design condition corresponding to the design dry-bulb temperature and the mean coincident wet-bulb temperature
c_p = specific heat at constant pressure (J/kg·K)
c_v = specific heat at constant volume (J/kg·K)
D = mass diffusion coefficient (m^2/s)
$\bar{g}$,g = gravitational acceleration vector, scalar (9.81 m/s^2)
h = height of inlet jet from the floor (m)
ΔH = enthalpy difference between outdoor and indoor air (kJ/kg)
$\bar{j}$ = contaminant mass flux (kg/[m^2·s])
L = diffuser inlet height or width (m)
$\dot{m}$ = mass flow rate of air (kg/s)
M = molecular weight (g/mole)
$\hat{n}$ = surface unit normal
p = static pressure (Pa)
$\bar{q}$ = heat flux vector (W)
q''' = heat source strength (W/m^3)
Q'' = volumetric flow rate per unit area (m^3/[s·m^2])
t = time (s)
T = air temperature (K)
$\bar{\bar{T}}$ = stress tensor
ΔT = air temperature difference (°C or K)
$\bar{U}$ = velocity (m/s)
U = speed (m/s)
u = air velocity component (m/s)
V, v = volume (m^3)
W = humidity ratio (kg/kg)
WB/MDB = design condition corresponding to the design wet-bulb temperature and the mean coincident dry-bulb temperature

BACK TO PAGE ONE

Greek Symbols

α = thermal diffusivity (m^2/s)
β = thermal expansion coefficient (K^{-1})
ε = contaminant removal effectiveness
ε_t = thermal energy removal effectiveness
Φ = viscous dissipation term ($J/[kg \cdot m^2]$)
μ = absolute viscosity ($N \cdot s/m^2$)
ν = kinematics viscosity (m^2/s)
ρ = air density (kg/m^3)

Subscripts

c = contaminant
e = exhaust
i = directional element
r = room
s = supply

Dimensionless Parameters

Ar = Archimedes number ($g \cdot \beta \cdot \Delta T \cdot h/U^2$)
Gr = Grashof number ($g \cdot \beta \cdot \Delta T \cdot h^3/\nu^2$)
J* = revised jet momentum number ($Q'' \cdot U_j/[g \cdot h]$)
Re = Reynolds number ($U \cdot L/\nu$)

REFERENCES

ASHRAE. 1996. *1996 ASHRAE handbook—HVAC systems and equipment*. Atlanta: American Society of Heating, Refrigerating and Air-Conditioning Engineers Inc.

ASHRAE. 1997. *1997 ASHRAE handbook—Fundamentals*. Atlanta: American Society of Heating, Refrigerating and Air-Conditioning Engineers Inc.

ASHRAE. 1989. *ANSI/ASHRAE Standard 62-1989, Ventilation for acceptable indoor air quality*. Atlanta: American Society of Heating, Refrigerating and Air-Conditioning Engineers Inc.

Baker, A.J., P.T. Williams, and R.M. Kelso. 1994. Numerical calculation of room air motion—Part 1: Math, physics, and CFD modeling. *ASHRAE Transactions* 100(1): 514-530.

Baker, A.T., R.M. Kelso, E.B. Gordon, S. Roy, and E.G., Schaub. 1997. Computational fluid dynamics: A two-edged sword. *ASHRAE Journal* 39(8): 51-58.

Chen, Q. 1997. Computational fluid dynamics for HVAC: Successes and failures. *ASHRAE Transactions* 103(1): 178-187.

Chen, Y.C., Y. Zhang, and E.M. Barber. 1995. A new mathematical model of particle size distribution for swine building dust. *ASHRAE Transactions* 101(2):1169-1178.

Chow, W.K., and W.Y. Fung. 1997. Experimental studies on the air flow characteristics of spaces with mechanical ventilation. *ASHRAE Transactions* 103(1): 31-41.

Gebhart, B., Y. Jaluria, T.L. Mahajan, and B. Sammakia. 1988. *Buoyancy-induced flows and transport*. New York: Hemisphere Publishing Corporation.

Heiselberg, P. 1996. Room Air and contaminant distribution in mixing ventilation. *ASHRAE Transactions* 102(2): 332-339.

Hoff, S.J., J. Li, and L. Tsao. 1995. Simulated and measured effect of rectangular obstructions on carbon dioxide gas dispersion in a scaled swine building. *ASAE Transactions* 38(5):1519-1532.

Irwin, D.R., and R.W. Besant. 1994. Contaminant removal effectiveness in a model barn using a displacement ventilation system and a conventional supply slot ventilation system. *ASHRAE Transactions* 100(2): 1021-1033.

Johnson, A.B., R.W. Besant, and G.J. Schoenau. 1995. Design of multi-coil run-around heat exchanger systems for ventilation air heating and cooling. *ASHRAE Transactions* 101(2): 967-978.

Johnson, A.B., C.J. Simonson, and R.W. Besant. 1998. Uncertainty analysis in the testing of air-to-air heat/energy exchangers installed in buildings. *ASHRAE Transactions* 104(1).

Kato, S., S. Murakami, and Y. Knodo. 1994. Numerical simulation of two-dimensional room airflow with and without buoyancy by means of ASM. *ASHRAE Transactions* 100(1): 238-255.

Kays, W.M. 1994. Turbulent Prandtl number—Where are we? *ASME Heat Transfer*, 116: 284-295.

Murakami, S., S. Kato, and Y. Suyama. 1990. Numerical study of flow and contaminant diffusion fields as affected fields by flow obstacles in conventional-flow-type clean room. *ASHRAE Transactions* 96(2): 343-355.

Panton, R. 1984. *Incompressible flow*. New York: John Wiley and Sons.

Simonson, C.J., and R.W. Besant. 1997. Heat and moisture transfer in desiccant coated rotary energy exchangers: Part II—Validation and sensitivity studies. *Int. J. HVAC&R Research*, 3(4): 351-368.

Simonson C.J., D.L. Ciepliski, and R.W. Besant. 1998. Determining the performance of energy wheels: Part II—Experimental data and numerical validation. *ASHRAE Transactions* 104(2).

Simonson, C.J., and R.W. Besant. 1998. Heat and moisture transfer in energy wheels during sorption, condensation and frosting conditions. *ASME J. Heat Transfer*.

Weathers, J.W., and J.D. Spitler. 1993. A comparative study of room airflow: Numerical prediction using computational fluid dynamics and full-scale experimental measurements. *ASHRAE Transactions* 99(2): 144-157.

Zhang J.S., L.L. Christianson, G.J. Wu, and G.L. Riskowski. 1992. Detailed measurements of room air distribution for evaluating numerical simulation models. *ASHRAE Transactions* 98(1): 58-65.